ELSEVIER

Contents lists available at ScienceDirect

Journal of Organometallic Chemistry

journal homepage: www.elsevier.com/locate/jorganchem





Chemical reduction of indenocorannulene: A two-electron addition stop

Yikun Zhu^a, Zheng Zhou^{a,b}, Zheng Wei^a, Marina A. Petrukhina^{a,*}

- ^a Department of Chemistry, University at Albany, State University of New York, Albany, NY, 12222, USA
- ^b School of Materials Science and Engineering, Tongji University, Shanghai 201804, China

ARTICLE INFO

Keywords: Indenocorannulene Bowl-shaped PAH Chemical reduction X-ray diffraction Alkali metals DFT calculation

ABSTRACT

Chemical reduction behavior of the indenyl-fused corannulene bowl, monoindenocorannulene (1), was investigated using two alkali metals with different binding abilities, namely Na and Rb. The sodium-induced reaction in THF in the presence of 18-crown-6 ether afforded a solvent-separated ion product, $[Na^+(18-crown-6)(THF)_2]_2[1^2^-]$. THF (2-THF), which enabled structural evaluation of the "naked" dianion. The controlled addition of the secondary ligand in rubidium-induced reduction reactions allowed modulation of metal coordination and solid-state packing of the doubly-reduced indenocorannulene. Two products with different topologies and metal ion binding, $[Rb^+(18-crown-6)]_2[1^2^-]$. THF (3-THF) and $[Rb^+(18-crown-6)]_Rb^+(18-crown-6)_0.5][1^2^-]$. 4THF (4-4THF), were isolated and characterized crystallographically. A direct comparison of 1 and 1^{2^-} using DFT calculation methods provided insights into consequences of two-fold reduction. The significant change in aromaticity was revealed by NICS calculations, while ACID plots showed a good agreement between the negative charge distribution patterns and the observed metal ion binding sites.

1. Introduction

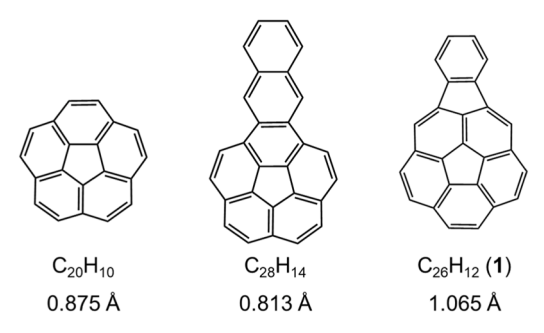
The discovery of the C₆₀-fullerene [1] opened up a plethora of investigations into larger fullerenes [2-4], fullerene derivatives [5-8] and fullerene-based materials [9-13], followed by a range of practical applications, including energy storage, superconductivity, sensing, etc. [14–18]. Rich redox chemistry of fullerenes revealed by electrochemical reduction [19-22] triggered extensive explorations of alkali-metal based products and their applications, including optical response, hydrogen storage, and superconductivity [23–26]. The M_3C_{60} (M=K, Rb, and Cs) products showed superior performance and potential as nontoxic and recyclable superconductors [27-30]. This discovery sparked special interest in exploration of bowl-shaped fragments of fullerenes, also referred to as buckybowls, carbon or π -bowls [31–34]. Buckybowls not only exhibit multi-step reduction properties but also provide easy access to open concave and convex faces [35–37]. Charging π -bowls with additional electrons generates a series of bowl-shaped anions with enhanced metal binding abilities. The smallest bowl-shaped corannulene (C₂₀H₁₀, Scheme 1), with the doubly degenerate LUMO, is able to accept up to four electrons [38,39]. The chemical reduction of corannulene was explored with all Group 1 metals, and products of all four reduction states were isolated and fully characterized [40]. The X-ray diffraction analysis revealed pronounced charge-dependent alkali metal

binding preferences [41–43], reduction induced σ -dimerization [44], as well as remarkable sandwich-type self-assemblies [45,46]. The very rich reduction and coordination chemistry of corannulene stimulated broad investigations of redox properties of bowl-shaped polycyclic aromatic hydrocarbons (PAHs) having different sizes, symmetry, and depth [47].

In 2018, the redox properties of a π -expanded corannulene derivative, naphthocorannulene (C₂₈H₁₄, Scheme 1), were tested with Na and Rb metals to reveal an ease of two-electron acceptance [48]. While incorporation of planar naphthalene group decreased the depth of the corannulene core, fusion of additional 5-membered rings further increased the core curvature, as illustrated by the whole family of indenocorannulenes [49]. The first member of this family, the monoindeno-fused bowl, indenocorannulene (C26H12, 1), exhibits a bowl depth increase at the corannulene core to 1.065 Å from 0.875 Å in corannulene [49]. The synthesis of 1 was first reported back in 1996, but the harsh reaction conditions led to a low yield and generation of by-products [50]. In 2003, the large-scale synthesis of 1 was developed using improved Suzuki-Heck coupling from monobromo-substituted corannulene [51]. The in situ chemical reduction of 1 with Li and K metals followed by NMR spectroscopy revealed fascinating dimerization/bond-cleavage processes for mono- and triply-reduced indenocorannulene [52]. In 2020, the first product of the mono-reduced 1°- radical-anion was isolated as the thermodynamically

E-mail address: mpetrukhina@albany.edu (M.A. Petrukhina).

^{*} Corresponding author.



Scheme 1. Depictions of corannulene, naphthocorannulene, and monoindenocorannulene (1) with their bowl depths.

stable dimer, $[\{Rb^+(18\text{-crown-6})\}_2(C_{26}H_{12}-C_{26}H_{12})^2-]\cdot 4THF$ [53], illustrating the role of curvature and strain on radical coupling processes of non-planar PAHs. Despite the revealed rich redox [52,53] and interesting coordination properties of indenocorannulene [54], no other reduction states of 1 have been isolated and crystallographically characterized.

Herein, we carried out chemical reduction of 1 with two alkali metals, Na and Rb, and isolated three new products of the doubly-reduced indenocorannulene. All products were fully characterized with single crystal X-ray diffraction, NMR and UV–Vis spectroscopic tools. The insights into their electronic structures and aromaticity were obtained with the help of DFT calculations.

2. Chemical reduction of 1 and crystallographic study

Chemical reduction of 1 was investigated with sodium and rubidium metals in THF in the presence of 18-crown-6 ether under argon atmosphere at room temperature. Starting from the initial light-yellow color, the reaction mixtures quickly changed to dark brown, followed by dark

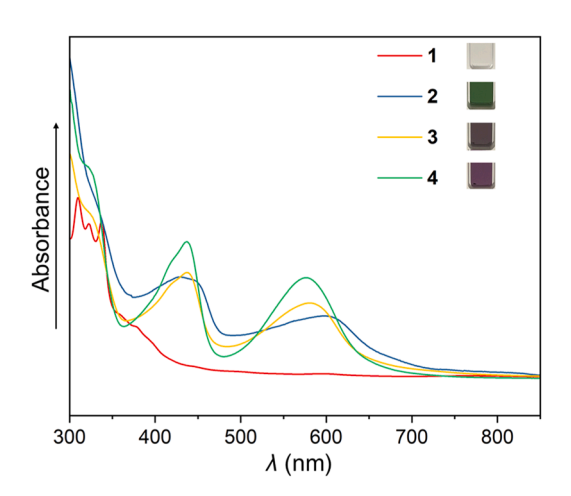


Fig. 1. UV-Vis absorption spectra of 1-4 in THF.

green with sodium metal and dark purple color with rubidium metal (Fig. 1, see ESI for more details).

Limited reaction time and controlled amount of a secondary ligand, 18-crown-6 ether, contributed to the preparation of the doubly-reduced indenocorannulene products with both metals (Scheme 2). Slow diffusion of anhydrous hexanes into the THF filtrates allowed the isolation of good quality single crystals in moderate yields. Their X-ray diffraction characterization revealed the formation of the doubly-reduced anions crystallized with the corresponding alkali metal countercations, namely $[Na^+(18\text{-crown-6})(THF)_2]_2[1^2]$ ·THF (2·THF), $[Rb^+(18\text{-crown-6})]_2[1^2]$ ·THF (3·THF) and $[Rb^+(18\text{-crown-6})][Rb^+(18\text{-crown-6})_{0.5}][1^2]$ ·4THF (4·4THF).

In the crystal structure of **2**, each Na⁺-ion wrapped by an axial 18-crown-6 molecule and two capped THF molecules remains solvent-separated from the $\mathbf{1}^{2-}$ anion (Fig. 2). Similar sodium-based compounds were also reported for corannulene and naphthocorannulene [55,48]. The isolation of the "naked" dianion in **2** enables the evaluation of the bowl core deformation upon addition of two electrons but without direct alkali metal binding influence (*vide infra*). The Na···O_{crown} distances (2.574(2)–2.884(2) Å) and Na···O_{THF} distances (2.259(3)–2.414 (7) Å) are close to the reported values [48,56,57]. In the solid-state structure of **2**, the C–H··· π interactions between one $\mathbf{1}^{2-}$ core and five surrounding counterions contribute to the 1D column packing (Fig. S11). The interstitial THF molecules fill the space between the adjacent columns without any notable interactions.

In the crystal structure of 3 (Fig. 3), Rb1 is η^5 -coordinated to the 5-membered ring of the indenyl group from the convex side of the bowl, with the Rb···C distances of 3.147(2)–3.300(2) Å. Additionally, Rb2 shows an endo- η^6 binding to the 6-membered ring of the same indenyl group, with the Rb···C distances ranging from 3.221(2) to 3.389(2) Å. Both Rb⁺-ions are capped by 18-crown-6 ether with the Rb1···O $_{crown}$ distances of 2.815(1)–3.079(1) Å and Rb2···O $_{crown}$ distances of 2.841 (1)–3.097(2) Å. All Rb···C distances and Rb···O distances are consistent

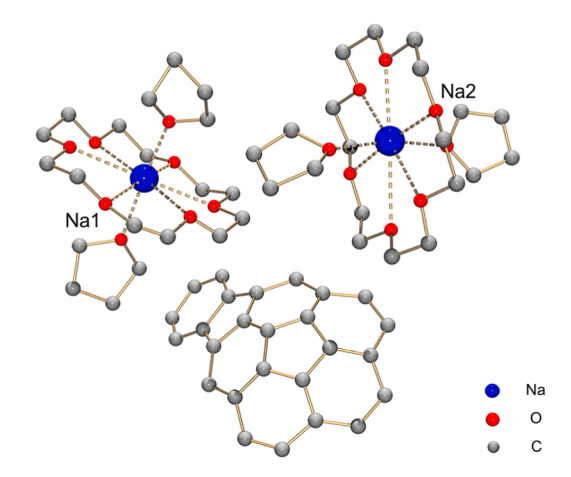
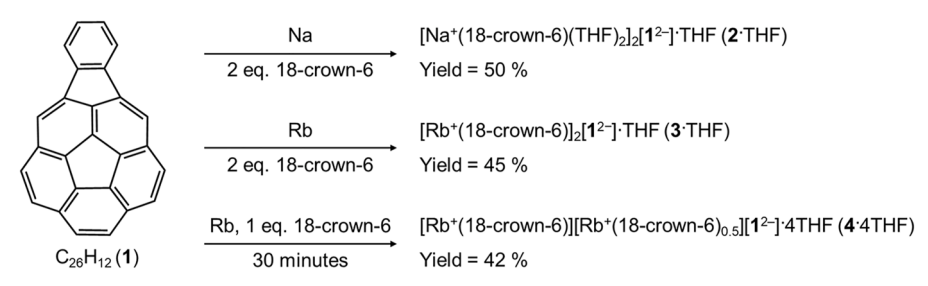


Fig. 2. Crystal structure of 2, ball-and-stick model. The H-atoms are omitted for clarity.



Scheme 2. Chemical reduction of 1 to afford 2-4.

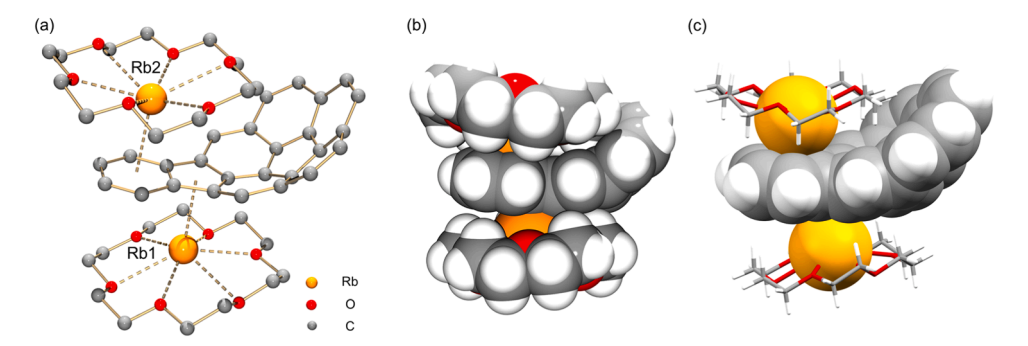


Fig. 3. Crystal structure of 3, (a) ball-and-stick (H-atoms are omitted for clarity), (b) space-filling, and (c) mixed models.

with the values previously reported [48,53,58]. In the solid-state structure of **3**, the C–H··· π interactions between the 18-crown-6 molecules and 1^{2-} core enable the formation of extended 2D layers (Fig. S12). The interstitial THF molecules fill the voids between the adjacent layers without notable interactions.

The insufficient amount of 18-crown-6 ether in the Rb-induced reduction of 1 led to the formation of a centrosymmetric tetranuclear complex 4 (Fig. 4). Similar aggregation was reported for the doubly-reduced indacenopicene, a constitutional isomer of 1, crystallized with Rb+ counterions wrapped by 18-crown-6 [59]. In the crystal structure of 4, Rb1 is placed inside the corannulene bowl and exhibits asymmetric coordination to the central five-membered ring and two six-membered rings (ring A and D) of 1^{2-} , with the Rb---C distances of 3.144(2)-3.618(2) Å. The two central Rb1 ions share one 18-crown-6 ether molecule (Rb---O_{crown}, 2.932(2)-3.118(2) Å), thus forming a tetranuclear unit capped by two external Rb2 ions. The outer Rb2 is $exo-\eta^5$ bound to the 5-membered ring of the indenyl group (Rb---C, 3.241(2)-3.424(2) Å) and is also capped by 18-crown-6 ether (Rb---O_{crown}, 2.835 (1)-3.011(1) Å).

In the solid-state structure of **4**, the $C-H\cdots\pi$ interactions are found between the terminal 18-crown-6 ether molecule and the adjacent $\mathbf{1}^{2-}$ core. As a result, an extended 2D "fishing net" structure is formed, where the interstitial THF molecules fill the voids as a caught "fish" without any secondary interactions (Fig. 5).

3. Deformation analysis of indenocorannulene

In comparison to the neutral parent 1 [49], the addition of two electrons results in the elongation of the C-C bonds of the corannulene core with a complementary reduction of the C-C bonds of the indenyl group. This is also accompanied by the bowl depth decrease in all three dianions (Table 1). Compared to the "naked" dianion in 2 (1.013(4) Å), the direct metal coordination increases the bowl depth to 1.056(3) Å in 3 and 1.027(4) Å in 4, with similar effect observed in the doubly-reduced naphthocorannulene [48]. As expected, when two Rb⁺ ions bind the indenyl group from opposite directions in 3, the changes of the indenyl C-C bonds were less pronounced compared to those in 4, but the bowl depth increase was more notable in 3. Besides, notable bond length alternation is observed for the five-membered ring of the indenyl group, with significant decrease of bond e (avg. 1.438 \mathring{A} in the dianions vs. 1.492 Å in 1) and elongation of bond g (avg. 1.482 Å in the dianions vs. 1.430 Å in 1, Table 1). A similar trend was observed for the doubly-reduced phenylenetetracene generated with rubidium and cesium metals used as the reducing agents [60]. Additionally, the bond distance alternation is also observed for bond h (avg. 1.453 Å in the dianions vs. 1.379 Å in 1) and i (avg. 1.408 Å in the dianions vs. 1.458 Å in 1). Notably, the C16 center between bond h and i is the position of σ -dimerization in the mono-reduced product [53].

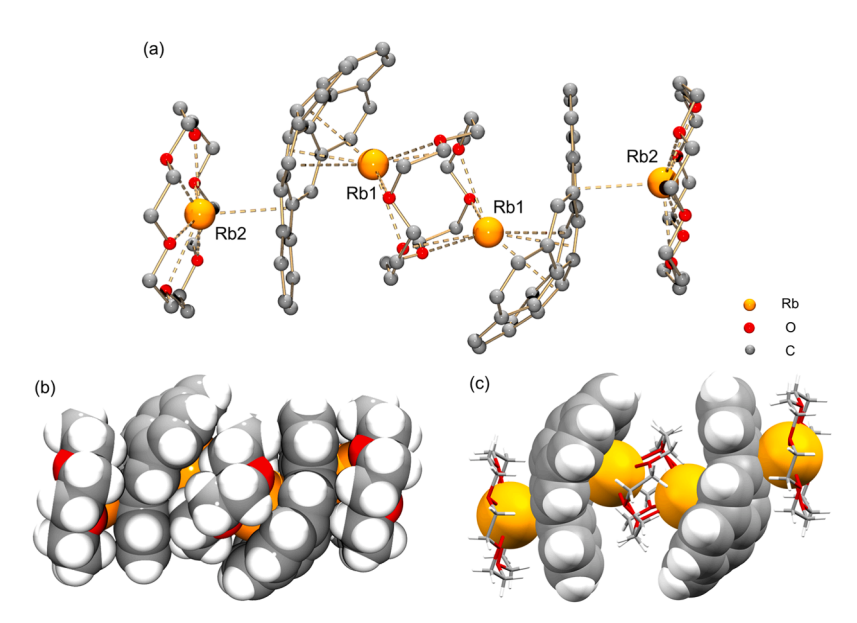


Fig. 4. Crystal structure of 4, (a) ball-and-stick (H-atoms are omitted for clarity), (b) space-filling, and (c) mixed models.

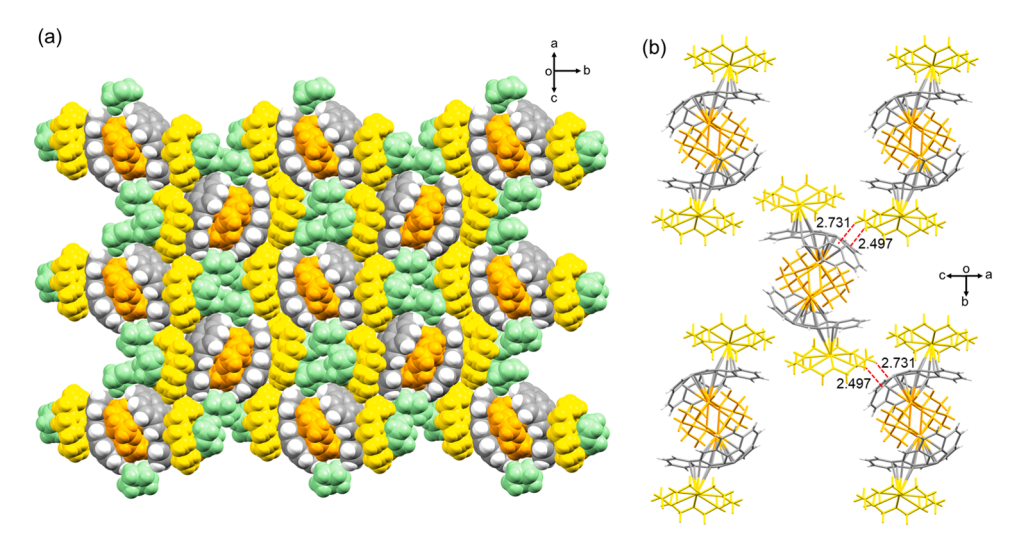
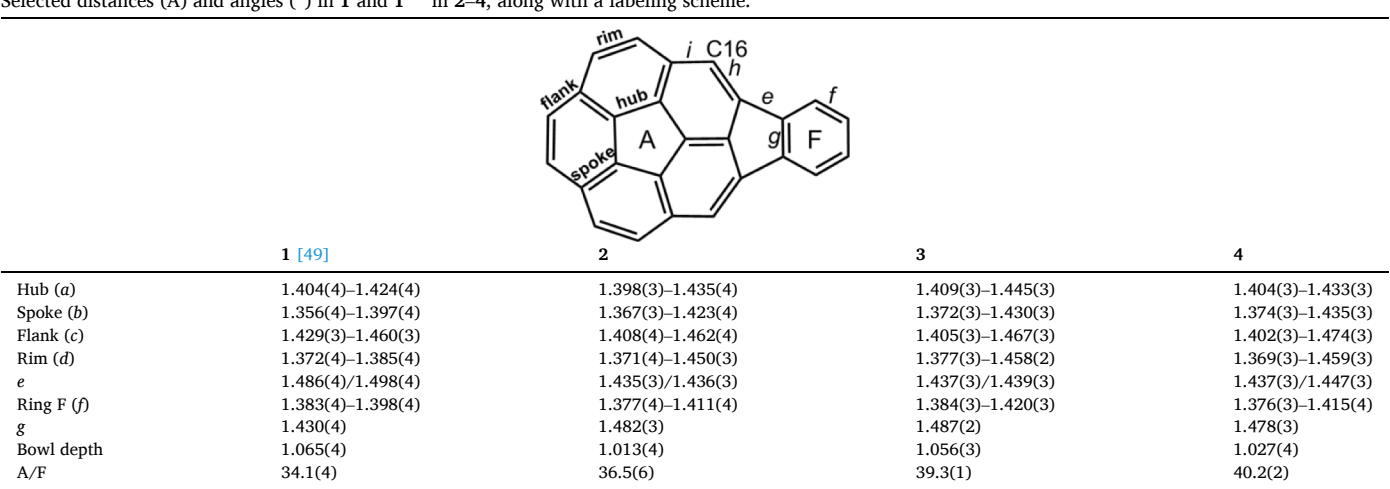


Fig. 5. (a) 2D layer packing of 4, space-filling model. The different cationic moieties are shown in different shades of orange. The interstitial THF molecules are shown in green. (b) $C-H\cdots\pi$ interactions (2.497(3)/2.731(3) Å) in 4, capped-stick model. The interstitial THF molecules are omitted for clarity.

Table 1 Selected distances (Å) and angles (°) in 1 and 1^{2-} in 2–4, along with a labeling scheme.



4. Computational investigation

In order to better understand the geometric and aromaticity changes stemming from a two-electron acquisition process, theoretical computation study was performed for neutral parent 1 and "naked" dianion 1^{2-} . The geometries were optimized using the B3LYP [61–64] function with def2-TZVP [65–69] basis set. The good match between the optimized structures and corresponding crystal structures justifies the adequacy of the selected functional (Table S6).

From the molecular electrostatic potential (MEP) maps of 1 (Fig. 6), two separate electron localization areas can be seen for the corannulene core and the indenyl group. As expected, the dianion has an overall enhanced electronic density which is localized at the center of the whole molecule (rings A, D, and E). This negative charge localization is in good agreement with the Rb $^+$ ion coordination found in 4. The optimized structure of Rb $_2$ –1 2 – showing the preferred binding sites for Rb $^+$ ions also agrees well with the experimentally observed coordination in 4 (Fig. S13). In 3, the metal coordination to the indenyl group was found less energetically favored, but it can be stabilized by the addition of two equivalents of 18-crown-6 ether.

The change in aromaticity was further analyzed with the magnetic nuclear independent chemical shift (NICS) calculations. The NICS(0)

values were calculated for natural aromaticity, while the NICS(1/-1) values were calculated to reduce the influence of σ -contamination and to illustrate the difference between the concave and convex surfaces (Fig. S14). Like corannulene and its derivatives, the neutral 1 also shows antiaromaticity of the central five-membered ring in the corannulene core but it is more pronounced (15.77 ppm in 1 ν s. 9.22 ppm in corannulene and 8.76 ppm in naphthocorannulene) [48]. The positive NICS (0) value for the five-membered ring E also reveals the lack of shared π -electrons between the corannulene core and indenyl group, further supporting the co-existence of two electron density areas in the MEP maps. Compared to the NICS(1) values, the overall larger NICS(-1) values reveal the higher π -electron density over the concave surface (Fig. 7a).

In the 1^{2-} anion, the aromaticity pattern is significantly different from the neutral parent. For the corannulene core, the central five-membered ring changes from antiaromatic to highly aromatic, and the outer six-membered rings change from aromatic to non-aromatic or even antiaromatic. On the other hand, the whole indenyl group becomes highly aromatic with large NICS values (Fig. 7b). This large diamagnetic ring current also generates severe deshielding of the indenyl group protons and leads to a large downfield shift, consistent with the reported $^1\mathrm{H}$ NMR results for the dianionic species [52]. The large increase of

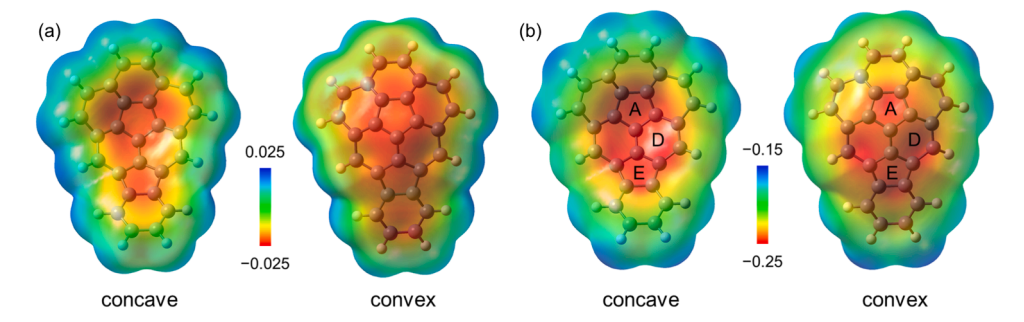


Fig. 6. MEP maps for (a) 1 and (b) 1^{2-} . The electron density is plotted at an isosurface value of 0.0004.

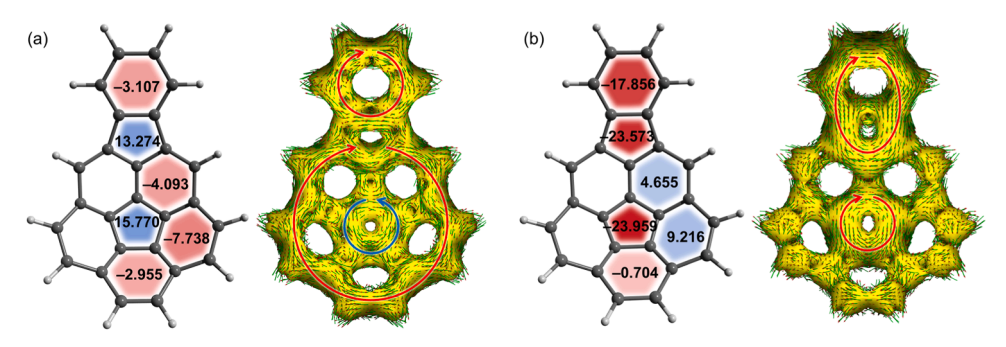


Fig. 7. Calculated NICS(0) values and ACID plots for (a) 1 and (b) 1^{2-} . The diatropic ring currents are highlighted in red and the paratropic ring currents are highlighted in blue.

aromaticity in rings A, E, and F enables stronger cation… π interactions, which is consistent with the observations in crystal structures of **3** and **4**. The anisotropy of the induced current (ACID) plots for **1** and **1**²⁻ shows good agreement to the calculated NICS values (Fig. 7). Moreover, the ring current difference between the concave and convex sides also illustrates the electron density difference from both directions (Fig. S15).

As a result of a two-electron addition to indenocorannulene core, the absolute NICS values of two five-membered rings were largely increased, revealing an elevated ring current density around these areas in accord with the increased total electron density observed in the MEP maps [70]. At the same time, although the ring current direction changes were observed for six-membered rings in the corannulene core, the current intensities remained comparable to the neutral 1.

5. Conclusion

In this work, the first products of the doubly-reduced indenocorannulene (1) were isolated and fully characterized. The use of two alkali metals having different coordination preferences, Na and Rb, and the adjustment of the metal-to-secondary-ligand ratio enabled the synthesis and crystallization of three distinct products with variable topologies and metal coordination patterns. This has allowed a detailed structural comparison of the "naked" dianion $\mathbf{1}^{2-}$ in $\mathbf{2}$ vs. parent $\mathbf{1}$ followed by the analysis of direct metal ion binding effects in 3 and 4. In 3, the steric effects and intramolecular C-H $\cdots\pi$ interactions involving 18-crown-6 supported the Rb⁺ ion coordination to the indenyl group. In 4, the insufficient amount of the secondary ligand led to a share of 18-crown-6 by two Rb⁺ ions and that facilitated the engagement of the corannulene core in metal binding. With the help of theoretical calculations, the effect of two-electron addition to 1 on molecular structure, electron distribution, and aromaticity was evaluated. The MEP maps of $\mathbf{1}^{2-}$ showed the electron density localization over the central part of the carbon framework which is in accord with the preferred Rb⁺ ion binding sites confirmed crystallographically. These results fill the gap in literature regarding the structure and alkali metal coordination of the doublyreduced indenocorannulene and should contribute to exploration and utilization of other curved π -expanded carbon systems in organometallic chemistry.

6. Experimental part

6.1. Materials and methods

All manipulations were carried out using break-and-seal and glovebox techniques under an atmosphere of argon [71]. Tetrahydrofuran (THF) and hexanes (Sigma Aldrich) were dried over Na/benzophenone and distilled prior to use. Tetrahydrofuran-d₈ (≥99.5 atom%D, Sigma Aldrich) was dried over NaK2 alloy and vacuum-transferred. Sodium (99.9%), rubidium (99.5%), and 18-crown-6 ether (99%) were purchased from Sigma Aldrich and used as received. C26H12 (1) was prepared according to the previously reported procedures [51] and sublimed at 190 °C prior to use. The UV-Vis absorption spectra were recorded on a Shimadzu UV-2600i UV-Vis spectrophotometer. The ¹H NMR spectra were recorded on a Bruker Ascend-500 spectrometer (500 MHz for 1 H). Chemical shifts (δ) are reported in parts per million (ppm) and referenced to the resonances of the corresponding solvent used. The extreme air- and moisture sensitivity of crystals 2-4, along with the presence of loosely-bound and interstitial THF molecules, prevented obtaining elemental analysis data.

6.2. $[Na^+(18\text{-}crown-6)(THF)_2]_2[C_{26}H_{12}^{2-}] \cdot THF (2 \cdot THF)$

THF (2.0 mL) was added to a customized glass system containing excess Na metal (3.0 mg, 0.130 mmol), 18-crown-6 ether (8 mg, 0.033 mmol) and 1 (5 mg, 0.015 mmol). The reaction mixture was stirred at 25 $^{\circ}\text{C}$ under argon for 24 h. The initial yellow color (neutral ligand) has changed to dark brown in 25 min, followed by dark green in 50 min and remained the same color until the reaction was stopped. The mixture was filtered after 24 h, and the green filtrate was layered with 1.5 mL of anhydrous hexanes. The ampule was sealed under argon and stored at 5

°C. After 7 days, black needle-shaped crystals deposited in the ampule. Yield: 10 mg, 50%. UV–Vis (THF): $\lambda_{\rm max}$ 445, 604 nm. $^{1}{\rm H}$ NMR (THF- $d_{\rm 8}$, ppm, 25 °C): δ = 4.90 (2H, 1^{2} –), 5.27–5.29 (2H, 1^{2} –), 5.51 (2H, 1^{2} –), 5.61–5.63 (2H, 1^{2} –), 6.76–6.77 (2H, 1^{2} –), 7.78–7.80 (2H, 1^{2} –).

6.3. $[Rb^+(18\text{-}crown-6)]_2[C_{26}H_{12}^2] \cdot THF$ (3.THF)

THF (2.0 mL) was added to a customized glass system containing excess Rb metal (3.0 mg, 0.035 mmol), 18-crown-6 ether (8 mg, 0.033 mmol) and 1 (5 mg, 0.015 mmol). The reaction mixture was stirred at 25 °C under argon for 1 h. The initial yellow color (neutral ligand) has changed to dark brown in 5 min, followed by greenish purple in 15 min and remained the same color until the reaction was stopped. The mixture was filtered after 1 h, and the purple filtrate was layered with 1.5 mL of anhydrous hexanes. The ampule was sealed under argon and stored at 5 °C. After 7 days, black block-shaped crystals formed in the ampule. Yield: 8 mg, 45%. UV–Vis (THF): $\lambda_{\rm max}$ 449, 590 nm. ¹H NMR (THF- d_8 , ppm, 25 °C): δ = 5.46 (2H, 1²⁻), 5.57 (2H, 1²⁻), 5.71–5.73 (2H, 1²⁻), 5.85–5.87 (2H, 1²⁻), 6.86–6.88 (2H, 1²⁻), 7.92–7.94 (2H, 1²⁻).

6.4. [Rb⁺(18-crown-6)][Rb⁺(18-crown-6)_{0.5}][1²⁻]·4THF (4·4THF)

THF (2.0 mL) was added to a customized glass system containing excess Rb metal (3.0 mg, 0.035 mmol), 18-crown-6 ether (4 mg, 0.016 mmol) and 1 (5 mg, 0.015 mmol). The reaction mixture was stirred at 25 °C under argon for 30 min. The initial yellow color (neutral ligand) has changed to dark brown in 5 min, followed by dark purple in 10 min and remained the same color until the reaction was stopped. The mixture was filtered after 30 min, and the purple filtrate was layered with 1.5 mL of anhydrous hexanes. The ampule was sealed under argon and stored at 5 °C. After 7 days, purple block-shaped crystals deposited in the ampule. Yield: 7 mg, 42%. UV–Vis (THF): $\lambda_{\rm max}$ 449, 590 nm. $^{1}{\rm H}$ NMR (THF- $d_{\rm 8}$, ppm, 25 °C): δ = 5.46 (2H, 1^{2-}), 5.57 (2H, 1^{2-}), 5.71–5.73 (2H, 1^{2-}), 5.85–5.87 (2H, 1^{2-}), 6.86–6.88 (2H, 1^{2-}), 7.92–7.94 (2H, 1^{2-}).

6.5. Crystal structure determinations and refinement of 2-4

Single crystals of 2-4 were mounted on a MiTeGen 20 μ m sample aperture and cooled to 100(2) K using an Oxford Instruments Cryojet cryostat. Data collections were performed on a Bruker D8 VENTURE Xray diffractometer with a PHOTON 100 CMOS shutterless mode detector equipped with a Mo-target X-ray tube ($\lambda = 0.71073 \text{ Å}$) and a Cu-target Xray tube ($\lambda = 1.54178 \text{ Å}$). Diffraction data were collected with frames of 0.5° using ω and ϕ scans. Data reduction and integration were performed with the Bruker software package SAINT (version 8.38A) [72]. All data were corrected for absorption effects using the empirical methods as implemented in SADABS (version 2016/2) [73]. The structures were solved by SHELXT (version 2018/2) [74] and refined by full-matrix least-squares procedures using the Bruker SHELXTL (version 2019/2) [75] software package through the OLEX2 [76] graphical interface. All non-hydrogen atoms were refined anisotropically. All hydrogen atoms were included at calculated positions and refined as riders with $U_{iso}(H) = 1.2 U_{eq}(C)$. In 2, all five THF and two 18-crown-6 ether molecules were found to be disordered. In 4, two THF molecules were disordered. All disordered molecules were modeled with two orientations with their relative occupancies refined. The geometries of the disordered parts were restrained to be similar. The anisotropic displacement parameters of the disordered molecules were restrained to have the same U_{ij} components, with a standard uncertainty of 0.01 Å². In 3, the structure was refined as a 2-domain twin with a twin law of -10 0 0 1 0 0 0 -1 and the BASF value was refined to 0.166(3). Crystallographic data and details of the data collection and structure refinement are listed in Table S2.

Declaration of Competing Interest

The authors declare no conflict of interest.

Data availability

All data are provided as Supporting Information

Acknowledgements

Financial and instrumentational support of this work from the U.S. National Science Foundation, CHE-2003411 and MRI-1726724, is gratefully acknowledged by M. A. P.

Supplementary materials

Supplementary material associated with this article can be found, in the online version, at doi:10.1016/j.jorganchem.2023.122805.

References

- H.W. Kroto, J.R. Heath, S.C. O'Brien, R.F. Curl, R.E. Smalley, C₆₀: buckminsterfullerene, Nature 318 (1985) 162–163, https://doi.org/10.1038/ 318162a0.
- B.L. Zhang, C.Z. Wang, K.M. Ho, Structures of large fullerenes: C₆₀ to C₉₄, Chem. Phys. Lett. 193 (1992) 225–230, https://doi.org/10.1016/0009-2614(92)85659-X.
- [3] B.L. Zhang, C.Z. Wang, K.M. Ho, C.H. Xu, C.T. Chan, The geometry of large fullerene cages: C₇₂ to C₁₀₂, J. Chem. Phys. 98 (1993) 3095–3102, https://doi.org/ 10.1063/1.464084.
- [4] B.-C. Wang, H.-W. Wang, J.-C. Chang, H.-C. Tso, Y.-M. Chou, More spherical large fullerenes and multi-layer fullerene cages, J. Mol. Struct. Theochem. 540 (2001) 171–176, https://doi.org/10.1016/S0166-1280(00)00739-9.
- [5] I.E. Kareev, N.B. Shustova, I.V. Kuvychko, S.F. Lebedkin, S.M. Miller, O. P. Anderson, A.A. Popov, S.H. Strauss, O.V. Boltalina, Thermally stable perfluoroalkylfullerenes with the skew-pentagonal-pyramid pattern: C₆₀(C₂F₅)₄O, C₆₀(CF₃)₄O, and C₆₀(CF₃)₆, J. Am. Chem. Soc. 128 (2006) 12268–12280, https://doi.org/10.1021/ja063907r.
- [6] N.B. Shustova, B.S. Newell, S.M. Miller, O.P. Anderson, R.D. Bolskar, K. Seppelt, A. A. Popov, O.V. Boltalina, S.H. Strauss, Discovering and verifying elusive fullerene cage isomers: structures of C₂-p¹¹-(C₇₄-D_{3h})(CF₃)₁₂ and C₂-p¹¹-(C₇₈-D_{3h}(5)) (CF₃)₁₂, Angew. Chem. Int. Ed. 46 (2007) 4111–4114, https://doi.org/10.1002/anie.200604968.
- [7] P.A. Troshin, R.N. Lyubovskaya, Organic chemistry of fullerenes: the major reactions, types of fullerene derivatives and prospects for practical use, Russ. Chem. Rev. 77 (2008) 323, https://doi.org/10.1070/ RC2008v077n04ARFH003770
- [8] A.A. Yurkova, E.A. Khakina, S.I. Troyanov, A. Chernyak, L. Shmygleva, A. S. Peregudov, V.M. Martynenko, Y.A. Dobrovolskiy, P.A. Troshin, Arbuzov chemistry with chlorofullerene C₆₀Cl₆: a powerful method for selective synthesis of highly functionalized [60]fullerene derivatives, Chem. Commun. 48 (2012) 8916–8918, https://doi.org/10.1039/C2CC34338J.
- [9] N.B. Shustova, D.V. Perysikov, I.V. Kuvychko, Y.-S. Chen, M.A. Mackey, C. E. Coumbe, D.T. Heaps, B.S. Confait, T. Heine, J.P. Phillips, S. Stevenson, L. Dunsch, A.A. Popov, S.H. Strauss, O.V. Boltalina, Poly(perfluoroalkylation) of metallic nitride fullerenes reveals addition-pattern guidelines: synthesis and characterization of a family of Sc_{3n}@C₈₀CF₃)_n (n = 2-16) and their radical anions, J. Am. Chem. Soc. 133 (2011) 2672–2690, https://doi.org/10.1021/ja109462j.
- [10] D.E. Williams, E.A. Dolgopolova, D.C. Godfrey, E.D. Ermolaeva, P.J. Pellechia, A. B. Greytak, M.D. Smith, S.M. Avdoshenko, A.A. Popov, N.B. Shustova, Fulleretic well-defined scaffolds: donor-fullerene alignment through metal coordination and its effect on photophysics, Angew. Chem. Int. Ed. 55 (2016) 9070–9074, https://doi.org/10.1002/anie.201603584.
- [11] A.M. Rice, E.A. Dolgopolova, N.B. Shustova, Fulleretic materials: buckyball- and buckybowl-based crystalline frameworks, Chem. Mater. 29 (2017) 7054–7061, https://doi.org/10.1021/acs.chemmater.7b02245.
- [12] X. Liu, M. Kozlowska, T. Okkali, D. Wagner, T. Higashino, G. Brenner-Weiß, S. M. Marschner, Z. Fu, Q. Zhang, H. Imahori, S. Bräse, W. Wenzel, C. Wöll, L. Heinke, Photoconductivity in metal-organic framework (MOF) thin films, Angew. Chem. Int. Ed. 58 (2019) 9590–9595, https://doi.org/10.1002/anie.201904475.
- [13] S.I. Vasylevskyi, G. Raffy, S. Salentinig, A. Del Guerzo, K.M. Fromm, D.M. Bassani, Multifunctional anthracene-based ni-mof with encapsulated fullerenes: polarized fluorescence emission and selective separation of C₇₀ from C₆₀, ACS Appl. Mater. Interfaces 14 (2022) 1397–1403, https://doi.org/10.1021/acsami.1c19141.
- [14] F. Diederich, M. Gómez-López, Supramolecular fullerene chemistry, Chem. Soc. Rev. 28 (1999) 263–277, https://doi.org/10.1039/A804248I.
- [15] F. Wudl, Fullerene materials, J. Mater. Chem. 12 (2002) 1959–1963, https://doi. org/10.1039/B201196D.

- [16] S. Margadonna, K. Prassides, Recent advances in fullerene superconductivity, J. Solid State Chem. 168 (2002) 639–652, https://doi.org/10.1006/ issr 2002 9762
- [17] S. Bosi, T. Da Ros, G. Spalluto, M. Prato, Fullerene derivatives: an attractive tool for biological applications, Eur. J. Med. Chem. 38 (2003) 913–923, https://doi.org/ 10.1016/j.ejmech.2003.09.005.
- [18] C. Thilgen, F. Diederich, Structural aspects of fullerene chemistry A journey through fullerene chirality, Chem. Rev. 106 (2006) 5049–5135, https://doi.org/ 10.1021/cr0505371.
- [19] F. Zhou, C. Jehoulet, A.J. Bard, Reduction and electrochemistry of fullerene C₆₀ in liquid ammonia, J. Am. Chem. Soc. 114 (1992) 11004–11006, https://doi.org/ 10.1021/ja00053a072
- [20] Q. Xie, E. Perez-Cordero, L. Echegoyen, Electrochemical detection of C₆₀⁻ and C₇₀⁻: enhanced stability of fullerides in solution, J. Am. Chem. Soc. 114 (1992) 3978–3980, https://doi.org/10.1021/ja00036a056.
- [21] T.F. Guarr, M.S. Meier, V.K. Vance, M. Clayton, Electrochemistry of the C₆₀H₂ fullerene, J. Am. Chem. Soc. 115 (1993) 9862–9863, https://doi.org/10.1021/ia00074a088.
- [22] A.L. Balch, D.A. Costa, W.R. Fawcett, K. Winkler, Electronic communication in fullerene dimers. Electrochemical and electron paramagnetic resonance study of the reduction of C₁₂₀O, J. Phys. Chem. 100 (1996) 4823–4827, https://doi.org/ 10.1021/jn953144m.
- [23] A. Zak, Y. Feldman, V. Lyakhovitskaya, G. Leitus, R. Popovitz-Biro, E. Wachtel, H. Cohen, S. Reich, R. Tenne, Alkali metal intercalated fullerene-like MS₂ (M = W, Mo) nanoparticles and their properties, J. Am. Chem. Soc. 124 (2002) 4747–4758, https://doi.org/10.1021/ja012060q.
- [24] K.R.S. Chandrakumar, S.K. Ghosh, Alkali-metal-induced enhancement of hydrogen adsorption in C₆₀ fullerene: An ab initio study, Nano Lett. 8 (2008) 13–19, https:// doi.org/10.1021/nl071456i.
- [25] N. Kosar, H. Tahir, K. Ayub, T. Mahmood, DFT studies of single and multiple alkali metals doped C₂₄ fullerene for electronics and nonlinear optical applications, J. Mol. Graph. Model. 105 (2021), 107867, https://doi.org/10.1016/j. jmgm.2021.107867.
- [26] R.K. Sahoo, B. Chakraborty, S. Sahu, Reversible hydrogen storage on alkali metal (Li and Na) decorated C₂₀ fullerene: a density functional study, Int. J. Hydrog. Energy. 46 (2021) 40251–40261, https://doi.org/10.1016/j. iihvdene.2021.09.219.
- [27] L. Degiorgi, E.J. Nicol, O. Klein, G. Grüner, P. Wachter, S.-M. Huang, J. Wiley, R. B. Kaner, Optical properties of the alkali-metal-doped superconducting fullerenes: K₃C₆₀ and Rb₃C₆₀, Phys. Rev. B. 49 (1994) 7012–7025, https://doi.org/10.1103/PhysRavB 49 7012
- [28] V. Buntar, F.M. Sauerzopf, H.W. Weber, Lower critical fields of alkali-metal-doped fullerene superconductors, Phys. Rev. B. 54 (1996) R9651–R9654, https://doi.org/ 10.1103/PhysRevB.54.R9651.
- [29] O. Zhou, Q. Zhu, J.E. Fischer, N. Coustel, G.B.M. Vaughan, P.A. Heiney, J. P. McCauley, A.B. Smith, Compressibility of M₃C₆₀ fullerene superconductors: relation between T_c and lattice parameter, Science 255 (1992) 833–835, https://doi.org/10.1126/science.255.5046.833
- [30] H.H. Wang, J.A. Schlueter, A.C. Cooper, J.L. Smart, M.E. Whitten, U. Geiser, K. D. Carlson, J.M. Williams, U. Welp, J.D. Dudek, M.A. Caleca, Fullerene derivatives and fullerene superconductors, J. Phys. Chem. Solids. 54 (1993) 1655–1666, https://doi.org/10.1016/0022-3697(93)90279-Z.
- [31] Y.-T. Wu, J.S. Siegel, Aromatic molecular-bowl hydrocarbons: Synthetic derivatives, their structures, and physical properties, Chem. Rev. 106 (2006) 4843–4867, https://doi.org/10.1021/cr050554q.
- [32] V.M. Tsefrikas, L.T. Scott, Geodesic polyarenes by flash vacuum pyrolysis, Chem.
- Rev. 106 (2006) 4868–4884, https://doi.org/10.1021/cr050553y.

 [33] A. Sygula, Chemistry on a half-shell: synthesis and derivatization of buckybowls, Eur. J. Org. Chem. 2011 (2011) 1611–1625, https://doi.org/10.1002/
- [34] C. Dubceac, A.S. Filatov, A.V. Zabula, A.Yu. Rogachev, M.A. Petrukhina, Functionalized corannulene carbocations: a structural overview, Chem. – Eur. J. 21 (2015) 14268–14279, https://doi.org/10.1002/chem.201500697.
- [35] M.A. Petrukhina, L.T. Scott, Coordination chemistry of buckybowls: from corannulene to a hemifullerene, Dalton Trans. (2005) 2969–2975, https://doi.org/ 10.1039/B504317D
- [36] M.A. Petrukhina, Coordination of buckybowls: the first concave-bound metal complex, Angew. Chem. Int. Ed. 47 (2008) 1550–1552, https://doi.org/10.1002/ pxis.20070478.
- [37] A.S. Filatov, M.A. Petrukhina, Probing the binding sites and coordination limits of buckybowls in a solvent-free environment: experimental and theoretical assessment, Coord. Chem. Rev. 254 (2010) 2234–2246, https://doi.org/10.1016/j.
- [38] A. Ayalon, M. Rabinovitz, P.-C. Cheng, L.T. Scott, Corannulene tetraanion: a novel species with concentric anionic rings, Angew. Chem. Int. Ed. Engl. 31 (1992) 1636–1637, https://doi.org/10.1002/anie.199216361.
- [39] M. Baumgarten, L. Gherghel, M. Wagner, A. Weitz, M. Rabinovitz, P.-C. Cheng, L. T. Scott, Corannulene reduction: spectroscopic detection of all anionic oxidation states, J. Am. Chem. Soc. 117 (1995) 6254–6257, https://doi.org/10.1021/io0138-013
- [40] Z. Zhou, M.A. Petrukhina, Planar, curved and twisted molecular nanographenes: reduction-induced alkali metal coordination, Coord. Chem. Rev. 486 (2023), 215144, https://doi.org/10.1016/j.ccr.2023.215144.
- [41] A.S. Filatov, N.J. Sumner, S.N. Spisak, A.V. Zabula, A.Yu. Rogachev, M. A. Petrukhina, Jahn–Teller effect in circulenes: x-ray diffraction study of coronene

- and corannulene radical anions, Chem. Eur. J. 18 (2012) 15753–15760, https://doi.org/10.1002/chem.201202026.
- [42] S.N. Spisak, A.V. Zabula, M.V. Ferguson, A.S. Filatov, M.A. Petrukhina, Naked" mono- and dianions of corannulene with lithium counterions, Organometallics 32 (2013) 538–543, https://doi.org/10.1021/om300998p.
- [43] S.N. Spisak, A.V. Zabula, A.S. Filatov, M.A. Petrukhina, Self-assembly of charged corannulene with cesium ions: always in the bowl, J. Organomet. Chem. 784 (2015) 69–74, https://doi.org/10.1016/j.jorganchem.2014.08.021.
- [44] A.Yu. Rogachev, M. Alkan, J. Li, S. Liu, S.N. Spisak, A.S. Filatov, M.A. Petrukhina, Mono-reduced corannulene: to couple and not to couple in one crystal, Chem. – Eur. J. 25 (2019) 14140–14147, https://doi.org/10.1002/chem.201902992.
- [45] A.V. Zabula, A.S. Filatov, S.N. Spisak, A.Yu. Rogachev, M.A. Petrukhina, A main group metal sandwich: five lithium cations jammed between two corannulene tetraanion decks, Science 333 (2011) 1008–1011, https://doi.org/10.1126/ science 1208686
- [46] A.V. Zabula, S.N. Spisak, A.S. Filatov, A. Yu. Rogachev, R. Clérac, M.A. Petrukhina, Supramolecular trap for a transient corannulene trianion, Chem. Sci. 7 (2016) 1954–1961, https://doi.org/10.1039/C5SC04385A.
- [47] M.A. Petrukhina, From corannulene to larger carbon bowls: are they better for multiple metal encapsulation? Dalton Trans. 48 (2019) 5125–5130, https://doi. org/10.1039/C9DT00424F.
- [48] Z. Zhou, S.N. Spisak, Q. Xu, A.Yu. Rogachev, Z. Wei, M. Marcaccio, M. A. Petrukhina, Fusing a planar group to a π-bowl: electronic and molecular structure, aromaticity and solid-state packing of naphthocorannulene and its anions, Chem. Eur. J. 24 (2018) 3455–3463, https://doi.org/10.1002/chem.201705814.
- [49] B.D. Steinberg, E.A. Jackson, A.S. Filatov, A. Wakamiya, M.A. Petrukhina, L. T. Scott, Aromatic π-systems more curved than C₆₀. The complete family of all indenocorannulenes synthesized by iterative microwave-assisted intramolecular arylations, J. Am. Chem. Soc. 131 (2009) 10537–10545, https://doi.org/10.1021/ja9031852.
- [50] A.K. Rai, Annulated and polysubstituted corannulenes: on the way to deeper bowls, M.S., n.d. https://www.proquest.com/pqdtglobal/docview/304330862/abstra ct/6ED8D62EACBE4E12PQ/1 (accessed February 24, 2023).
- [51] H.A. Wegner, L.T. Scott, A. de Meijere, A new Suzuki-Heck-type coupling cascade: indeno[1,2,3]-annelation of polycyclic aromatic hydrocarbons, J. Org. Chem. 68 (2003) 883–887, https://doi.org/10.1021/jo020367h.
- [52] I. Aprahamian, R.E. Hoffman, T. Sheradsky, D.V. Preda, M. Bancu, L.T. Scott, M. Rabinovitz, A four-step alternating reductive dimerization/bond cleavage of indenocorannulene, Angew. Chem. Int. Ed. 41 (2002) 1712–1715, https://doi.org/ 10.1002/1521-3773(20020517)41:10<1712::AID—ANIE1712>3.0.CO;2-1.
- [53] A.Y. Rogachev, Y. Zhu, Z. Zhou, S. Liu, Z. Wei, M.A. Petrukhina, Dimerization of indenocorannulene radicals: imposing stability through increasing strain and curvature, Org. Chem. Front. 7 (2020) 3591–3598, https://doi.org/10.1039/ D0O000686F.
- [54] A.S. Filatov, A.Yu. Rogachev, E.A. Jackson, L.T. Scott, M.A. Petrukhina, Increasing the curvature of a bowl-shaped polyarene by fullerene-like η²-complexation of a transition metal at the interior of the convex surface, Organometallics 29 (2010) 1231–1237, https://doi.org/10.1021/om100024c.
- [55] A.V. Zabula, S.N. Spisak, A.S. Filatov, V.M. Grigoryants, M.A. Petrukhina, How charging corannulene with one and two electrons affects its geometry and aggregation with sodium and potassium cations, Chem. – Eur. J. 18 (2012) 6476–6484, https://doi.org/10.1002/chem.201200416.
- [56] Z. Zhou, Z. Wei, Y. Tokimaru, S. Ito, K. Nozaki, M.A. Petrukhina, Stepwise reduction of azapentabenzocorannulene, Angew. Chem. Int. Ed. 58 (2019) 12107–12111, https://doi.org/10.1002/anie.201906748.
- [57] Z. Zhou, Y. Zhu, J.M. Fernández-García, Z. Wei, I. Fernández, M.A. Petrukhina, N. Martín, Stepwise reduction of a corannulene-based helical molecular nanographene with Na metal, Chem. Commun. 58 (2022) 5574–5577, https://doi. org/10.1039/D2CC00971D
- [58] M. Pennachio, Z. Zhou, Z. Wei, A. Tsybizova, R. Gershoni-Poranne, M. A. Petrukhina, Interplay of charge and aromaticity upon chemical reduction of pquinquephenyl with alkali metals, Organometallics (2023), https://doi.org/ 10.1021/acs.organomet.2c00583.
- [59] S.N. Spisak, J. Li, A.Yu. Rogachev, Z. Wei, O. Papaianina, K. Amsharov, A. V. Rybalchenko, A.A. Goryunkov, M.A. Petrukhina, From corannulene to indacenopicene: effect of carbon framework topology on aromaticity and reduction limits, Organometallics 35 (2016) 3105–3111, https://doi.org/10.1021/acs.organomet.6b00395.
- [60] T. Wombacher, R. Goddard, C.W. Lehmann, J.J. Schneider, Organometallic rubidium and cesium compounds of the 5,6;11,12-di-o-phenylene-tetracene dianion, Chem. Commun. 53 (2017) 7030–7033, https://doi.org/10.1039/ CZCCONDADY
- [61] A.D. Becke, A new mixing of Hartree–Fock and local density-functional theories, J. Chem. Phys. 98 (1993) 1372–1377, https://doi.org/10.1063/1.464304.
- [62] P.J. Stephens, F.J. Devlin, C.F. Chabalowski, M.J. Frisch, Ab initio calculation of vibrational absorption and circular dichroism spectra using density functional force fields, J. Phys. Chem. 98 (1994) 11623–11627, https://doi.org/10.1021/ i100096a001.
- [63] S.H. Vosko, L. Wilk, M. Nusair, Accurate spin-dependent electron liquid correlation energies for local spin density calculations: a critical analysis, Can. J. Phys. 58 (1980) 1200–1211, https://doi.org/10.1139/p80-159.
- [64] C. Lee, W. Yang, R.G. Parr, Development of the Colle-Salvetti correlation-energy formula into a functional of the electron density, Phys. Rev. B. 37 (1988) 785–789, https://doi.org/10.1103/PhysRevB.37.785.

- [65] F. Weigend, R. Ahlrichs, Balanced basis sets of split valence, triple zeta valence and quadruple zeta valence quality for H to Rn: design and assessment of accuracy, Phys. Chem. Chem. Phys. 7 (2005) 3297–3305, https://doi.org/10.1039/ B508541A.
- [66] B.P. Pritchard, D. Altarawy, B. Didier, T.D. Gibson, T.L. Windus, New basis set exchange: an open, up-to-date resource for the molecular sciences community, J. Chem. Inf. Model. 59 (2019) 4814–4820, https://doi.org/10.1021/acs. icim.9b00725.
- [67] T. Leininger, A. Nicklass, W. Küchle, H. Stoll, M. Dolg, A. Bergner, The accuracy of the pseudopotential approximation: non-frozen-core effects for spectroscopic constants of alkali fluorides XF (X = K, Rb, Cs), Chem. Phys. Lett. 255 (1996) 274–280, https://doi.org/10.1016/0009-2614(96)00382-X.
- [68] D. Feller, The role of databases in support of computational chemistry calculations, J. Comput. Chem. 17 (1996) 1571–1586, https://doi.org/10.1002/(SICI)1096-987X(199610)17:13<1571::AID-JCC9>3.0.CO;2-P.
- [69] T. Korona, M. Przybytek, B. Jeziorski, Time-independent coupled cluster theory of the polarization propagator. Implementation and application of the singles and doubles model to dynamic polarizabilities and van der Waals constants, Mol. Phys. 104 (2006) 2303–2316, https://doi.org/10.1080/00268970600673975.

- [70] C. Foroutan-Nejad, S. Shahbazian, P. Rashidi-Ranjbar, The electron density vs. NICS scan: a new approach to assess aromaticity in molecules with different ring sizes, Phys. Chem. Chem. Phys. 12 (2010) 12630–12637, https://doi.org/10.1039/ C004254D
- [71] N.V. Kozhemyakina, J. Nuss, M. Jansen, Demonstration of the "break-and-seal" approach to fullerides of complex cations at the example of KC₆₀(THF)₅·2THF, Z. Für Anorg. Allg. Chem. 635 (2009) 1355–1361, https://doi.org/10.1002/ 200200283
- [72] SAINT; Part of Bruker APEX3 Software Package (version 2017.3-0), Bruker AXS, (2017).
- [73] SADABS; Part of Bruker APEX3 Software Package (version 2017.3-0), Bruker AXS, (2017)
- [74] G.M. Sheldrick, SHELXT Integrated space-group and crystal-structure determination, Acta Crystallogr. Sect. A 71 (2015) 3–8, https://doi.org/10.1107/ S2052372314056270
- [75] G.M. Sheldrick, Crystal structure refinement with SHELXL, Acta Crystallogr C71 (2015) 3–8, https://doi.org/10.1107/S2053229614024218.
- [76] O.V. Dolomanov, L.J. Bourhis, R.J. Gildea, J.A.K. Howard, H. Puschmann, OLEX2: a complete structure solution, refinement and analysis program, J. Appl. Crystallogr. 42 (2009) 339–341, https://doi.org/10.1107/S0021889808042726.